Supplementary Materials

The Community Earth System Model

The Community Earth System Model (CESM1) is a global climate model that couples individual models including models of the Earth's atmosphere, ocean, land, and sea ice to provide a comprehensive representation of interacting Earth systems (Gent et al., 2011; Hurrell et al., 2013). In this work we utilize the CESM1 with two atmospheric configurations: 1) the Whole Atmosphere Community Climate Model (WACCM), and 2) the Community Atmosphere Model (CAM4). We also use the Community Aerosol and Radiation Model for Atmospheres (CARMA), which is a configurable sectional aerosol model included within the coupled framework of CESM1. Figure S1 illustrates the modeling framework.

CARMA

The Community Aerosol and Radiation Model for Atmospheres (CARMA) is a sectional aerosol microphysical model (English et al., 2011). Processes including aerosol nucleation, growth, settling, and sulfur chemistry are included (Turco et al., 1979; Toon et al., 1988; English et al., 2011). In this study, CARMA has been advectively coupled to CESM1(WACCM) to allow three-dimensional simulation of the evolving aerosol cloud (Mills et al., 2008; English et al., 2011; English et al., 2013). The specific sectional setup implemented here includes 35 aerosol size bins, ranging from 0.003 microns to 7 microns; each bin is included as a tracer within CESM1(WACCM). Aerosol heating is not included; nor are the radiative effects of volcanic ash. The effects of fine volcanic ash on climate and atmospheric circulation are small (Niemeier et al., 2009). However, aerosol heating of sulfates from tropical eruptions has been shown to strongly influence the dispersal of the sulfates (Aquila et al., 2012; Toohey et al., 2011). This effect may be tempered by the relatively high latitude of the Campanian Ignimbrite eruption.

WACCM

CESM1(WACCM) has a 1.9° × 2.5° horizontal resolution with 66 vertical levels that extend to ~140 km altitude. In the configuration used in this study, WACCM handles the representation of dynamics, atmospheric chemistry, physics, and coupling to the land and prescribed sea surface temperatures within CESM while CARMA handles only the sulfate aerosol microphysics. Please see Marsh et al. (2013) for full details on the standard configuration of CESM1(WACCM). In the configuration used here, the chemistry of CESM1(WACCM) has been specifically expanded to include the necessary sulfur chemistry for the accurate conversion of the volcanic SO_2 plume and other background sulfur sources (mainly OCS) into sulfate. The hydroxyl radical is the primary oxidant of SO_2, and thus the time evolution of the sulfate burden will depend on hydroxyl mixing ratios. We use pre-industrial hydroxyl mixing ratios; Murray et al. (2014) have shown that this assumption is likely valid for the Last Glacial Maximum. In the probable absence of significantly warmer or colder temperatures (Martrat et al., 2004) that would substantially influence the quantity of water in the atmosphere (Schmidt and Shindell, 2003), and thus hydroxyl production and SO_2 oxidation rates, our assumed pre-industrial hydroxyl concentrations (0.05 ppt) are unlikely to bias our results. Our model does not include a Quasi-Biennial Oscillation. The setup for the simulation of each volcanic injection is summarized in Supplementary Table 1.

Prescription of WACCM-CARMA results in CESM1(CAM4) under last glacial conditions

CESM1(CAM4) is the tropospheric atmospheric model within CESM1 and utilizes 26 vertical levels (extending to ~40 km altitude) with a horizontal resolution of 0.9° × 1.25°. We include boundary conditions appropriate for the last glacial period (see Brady et al., 2013 and Supplementary Table 2 for additional details). Figure S2 shows that our results are only modestly sensitive to the land surface dataset we use. To couple the results of CARMA to CESM1(CAM4), we calculate the optical properties of the aerosol cloud offline from the CARMA output (Neely et al., 2011; Neely et al., 2013). CARMA tracks the dry sulfate radius and mass only. Therefore, we first convert to wet aerosol mass and size by accounting for temperature and water activity (Tabazadeh et al., 1997; English et al., 2011). The aerosol wet effective radius is then used in Mie calculations to determine extinction and backscattering, as described by Neely et al. (2011). Finally, the radiative effects of the CARMA sulfate aerosol distributions and wet effective radii in four dimensions (space and time) are calculated within CESM by the CAM-RT radiative transfer scheme (Collins et al., 2006), during fully coupled simulations with last glacial paleogeography (Brady et al., 2013).

Ocean model

In our WACCM-CARMA simulations, to limit computational expense we use prescribed sea surface temperatures (including prescribed sea ice extent) based on a climatology derived from the results of Brady et al. (2013). The simulations with CESM1(CAM4) under last glacial conditions include the fully interactive Parallel Ocean Program (POP2) model (Smith et al., 2010; Gent et al., 2011).

Land dataset

The last glacial land surface dataset used in the simulations with CESM1(CAM4) is identical to that of Brady et al. (2013); we include PMIP3/CMIP5 last glacial maximum ice sheets that were produced by averaging three ice sheet reconstructions (Tarasov and Peltier, 2004; Argus and Peltier, 2010; Lambeck et al., 2010). The sensitivity of our results to the land surface dataset is illustrated in Figure S3.

GISP2 ice core

We calculate the sulfate deposition recorded in the GISP2 ice core using sulfate data from Zielinski et al. (1996) and the age model of Meese et al. (1997) as follows (see also Figure S4):

$$SO_4^{2-}\left[\frac{kg}{km^2}\right] = SO_4^{2-}\left[\frac{kg}{kg\ ice}\right] \times \rho_{ice}\left[\frac{kg\ ice}{m^3}\right] \times d\ [m] \times \left[\frac{1000000\ m^2}{km^2}\right].$$

With a concentration of volcanic SO_4^{2-} in the GISP2 core of $374 \times 10^{-9}\ \frac{kg}{kg\ ice}$ (Zielinski et al., 1996), and assuming ice density $\rho_{ice} = 916\ kg/m^3$, and depth $d = 0.2\ m$ (Figure S4), we calculate sulfate deposition of ~70 kg/m^2.

Hominid site data

We compiled a list of Neanderthal and anatomically modern human sites from Banks et al. (2008) and Higham et al. (2014) that yield radiocarbon age determinations that overlap within 2-σ uncertainty with the age of the Campanian Ignimbrite as estimated from the ice core age model (Meese et al., 1997; Fedele et al., 2008). We included both Mousterian and Châtelperronian sites from Higham et al. (2014) when plotting these sites in Figure 4 in the main text. The site names, locations, age determinations, and archaeological classifications are summarized in Supplementary Table 3.

Supplementary Table 1. Complete list of runs, including sensitivity tests.				
Model	**Scenario**	**Run name**	**# of runs**	**Description**
CARMA coupled to CESM1(WACCM)	50 Tg SO_2	CARMA_50	1	Sectional aerosol microphysics model (CARMA) advectively coupled to WACCM, with 66-level atmosphere extending to 140 km altitude and 1.9° × 2.5° horizontal resolution. Present-day geography and pre-industrial chemistry without anthropogenic emissions, and only CI volcanic emissions. Sulfur emissions between 39 °N to 41 °N and 13 °E to 15 °E, and distributed from 18 to 30 km altitude (with a peak at 24 km). Prescribed SSTs.
CARMA coupled to CESM1(WACCM)	200 Tg SO_2	CARMA_200	1	Identical to CARMA_50 but with 200 Tg SO_2.
CARMA coupled to CESM1(CAM4)	200 Tg SO_2	CARMA_200_LG	1	Sensitivity test. Identical emissions as in CARMA_200 but with last glacial conditions (185 ppm CO_2, 23.5 ka ice cover) and 26-level atmosphere (to ~40 km altitude) with 0.9° × 1.25° horizontal resolution.
CESM1(CAM4)	50 Tg SO_2	CESM_50_LG_1,2,3	3	Ensemble of three fully coupled simulations with last glacial conditions: 185 ppm CO_2, 23.5 ka ice cover. Aerosol forcing prescribed from run CARMA_50. Initialized from Brady et al. (2013) (their simulation years 1894, 1897, and 1900). 26-level atmosphere (to ~40 km altitude) with 0.9° × 1.25° horizontal resolution.
CESM1(CAM4)	200 Tg SO_2	CESM_200_LG_1,2,3	3	Ensemble with same conditions as CESM_50_LG_1,2,3 but with aerosol forcing from CARMA_200.
CESM1(CAM4)	0 Tg SO_2	CESM_control_LG_1,2,3	3	Control runs for ensemble simulations. Initialized from three different years from Brady et al. (2013).
CESM1(CAM4)	200 Tg SO_2	CESM_200_present	1	Sensitivity test. Aerosol forcing from CARMA_200 (identical to CESM_200_LG runs) but with present-day

				geography and initial climate. 26-level atmosphere (to ~40 km altitude) with 0.9° × 1.25° horizontal resolution.

Supplementary Table 2. Last Glacial Conditions
CO_2: 185 ppm
CH_4: 350 ppb
N_2O: 200 ppb
Orbital year: 21 ka
See Table 1 of Brady et al. (2013)

Supplementary Table 3. Neanderthal and Anatomically Modern Human sites

Site Name	**Latitude °N**	**Longitude °E**	**Final Boundary Age (years cal BP, 95% confidence interval)**		**Archaeological context**	**Reference**
Spy	50.47	4.67	41,210-37,830		Mousterian	Higham et al. (2014)
Mezmaiskaya	44.20	39.99	42,300-39,220		Mousterian	Higham et al. (2014)
Saint-Cesaire	45.76	-0.64	See Higham et al. (2014), Figure S4.		Châtelperronian	Higham et al. (2014)
Arcy-sur-Cure	47.59	3.75	See Higham et al. (2014), Figure S2.		Châtelperronian	Higham et al. (2014)
Le Moustier	44.99	1.05	See Higham et al. (2014), Figure S1.		Châtelperronian	Higham et al. (2014)
Site Name	**Latitude °N**	**Longitude °E**	**Age (cal BP years)**	**1-σ (years)**	**Archaeological context**	**Reference**
Arbreda	42.17	2.75	39160	700	Mousterian	Banks et al. (2008)
Arrillor	43.01	0.94	41900	1000	Mousterian	Banks et al. (2008)
Buzdujeni	48.17	27.3	39910	1400	Mousterian	Banks et al. (2008)
Cabezo Gordo	37.73	-0.95	39690	600	Mousterian	Banks et al. (2008)
Esquilleu	43.2	-4.6	39580	670	Mousterian	Banks et al. (2008)
Esquilleu	43.2	-4.6	41140	830	Mousterian	Banks et al. (2008)
Gorham's Cave	36.21	-5.35	39590	900	Mousterian	Banks et al. (2008)
Jarama	40.92	-3.33	37560	1800	Mousterian	Banks et al. (2008)
Las Fuentes	42.13	-0.41	40840	550	Mousterian	Banks et al. (2008)
Belvis	42.85	2.08	40110	1140	Châtelperronian	Banks et al. (2008)

Grotte du Renne	47.62	3.75	39580	750	Châtelperronian	Banks et al. (2008)
Grotte XVI	44.8	1.2	39700	1200	Châtelperronian	Banks et al. (2008)
Grotte XVI	44.8	1.2	42430	1670	Châtelperronian	Banks et al. (2008)
La Quina	45.82	0.45	40800	450	Châtelperronian	Banks et al. (2008)
Roc de Combe	44.75	1.35	41950	2000	Châtelperronian	Banks et al. (2008)
Stranska Skala	49.82	13.68	39640	770	Bohunician	Banks et al. (2008)
Stranska Skala	49.82	13.68	40830	990	Bohunician	Banks et al. (2008)
Bacho Kiro	42.93	25.42	39530	1150	Aurignacian	Banks et al. (2008)
Bacho Kiro	42.93	25.42	42080	1450	Aurignacian	Banks et al. (2008)
Beneito	38.7	-0.47	38660	1100	Aurignacian	Banks et al. (2008)
Caminade	44.87	1.25	40110	1100	Aurignacian	Banks et al. (2008)
Caminade	44.87	1.25	41320	1500	Aurignacian	Banks et al. (2008)
Castanet	45.03	1.18	39590	1100	Aurignacian	Banks et al. (2008)
Castillo	43.29	-3.97	41700	1800	Aurignacian	Banks et al. (2008)
Combe Sauniere	45.14	0.16	38850	850	Aurignacian	Banks et al. (2008)
Divje Babe	46	14.06	40210	700	Aurignacian	Banks et al. (2008)
Flageolet	44.82	0.58	38980	1100	Aurignacian	Banks et al. (2008)
Fumane	45.55	10.88	39700	347	Aurignacian	Banks et al. (2008)
Geissenklosterle	48.4	9.78	39660	310	Aurignacian	Banks et al. (2008)
Hohle Fels	48.37	9.73	39630	340	Aurignacian	Banks et al. (2008)
Hohlenstein Stadel	48.77	10.38	39420	310	Aurignacian	Banks et al. (2008)
Isturitz	43.37	-1.2	39830	560	Aurignacian	Banks et al. (2008)
Mochi	43.78	7.53	39890	800	Aurignacian	Banks et al. (2008)
Paglicci	41.67	15.58	39180	800	Aurignacian	Banks et al. (2008)
Pataud	44.9	0.38	39450	675	Aurignacian	Banks et al. (2008)
Roc de Combe	44.75	1.35	38300	1100	Aurignacian	Banks et al. (2008)
Romani	41.54	1.67	41540	920	Aurignacian	Banks et al. (2008)
Solutre	46.38	4.31	39440	360	Aurignacian	Banks et al. (2008)
Temnata	43.17	24.05	41140	1300	Aurignacian	Banks et al. (2008)
Trou Al Wesse	50.47	5.25	40900	1100	Aurignacian	Banks et al. (2008)
Vogelherd	47.95	10.07	38810	1100	Aurignacian	Banks et al. (2008)
Wildscheuer	50.4	8.17	39040	900	Aurignacian	Banks et al. (2008)

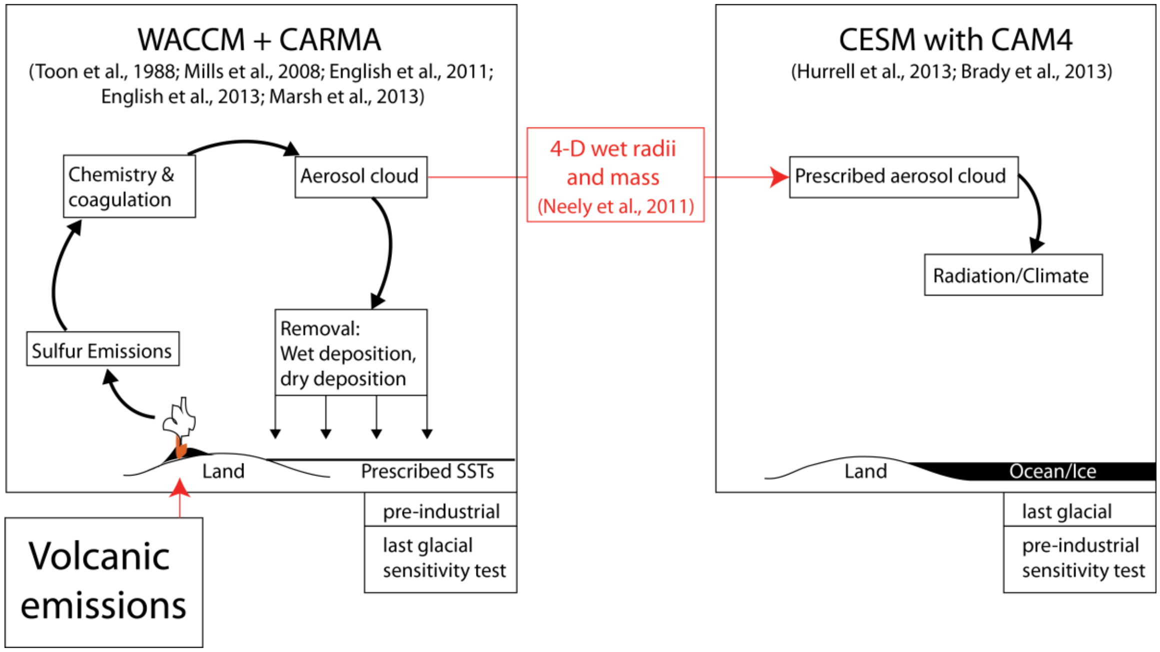

Figure S1. Schematic illustration of the modeling configuration.

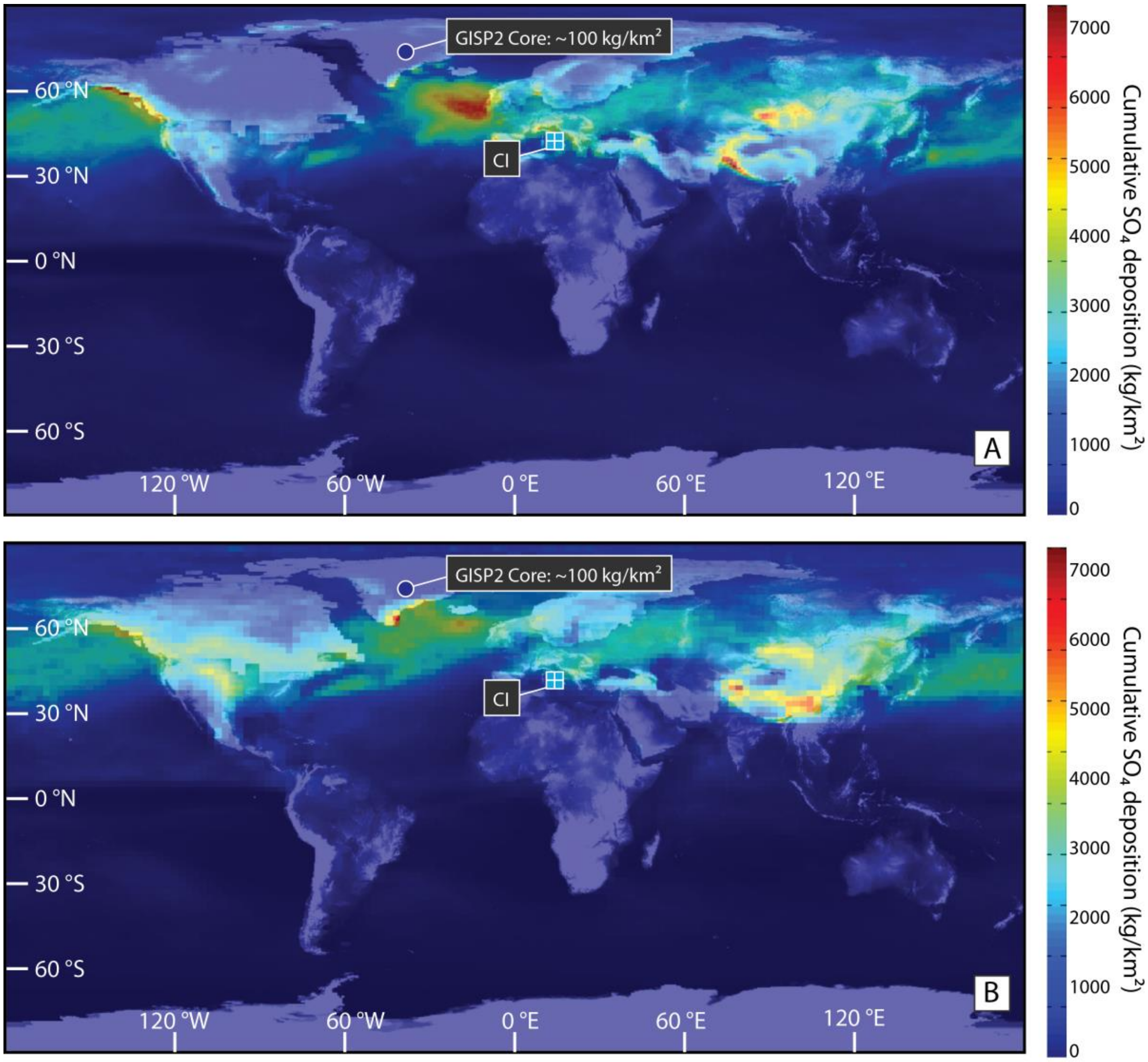

Figure S2. Sensitivity test comparing sulfate deposition for CARMA run with last glacial boundary conditions (panel A) vs. present-day boundary conditions (panel B). Both simulations include 200 Tg SO_2 emissions. The cumulative sulfate deposition is the total wet and dry deposition during the course of the five year simulations. The overall pattern of sulfate deposition is similar between the simulations; the differences are primarily controlled by shifts in precipitation that affect wet deposition. Sulfate deposition in Greenland in both these simulations exceeds deposition rates recorded in the GISP2 core.

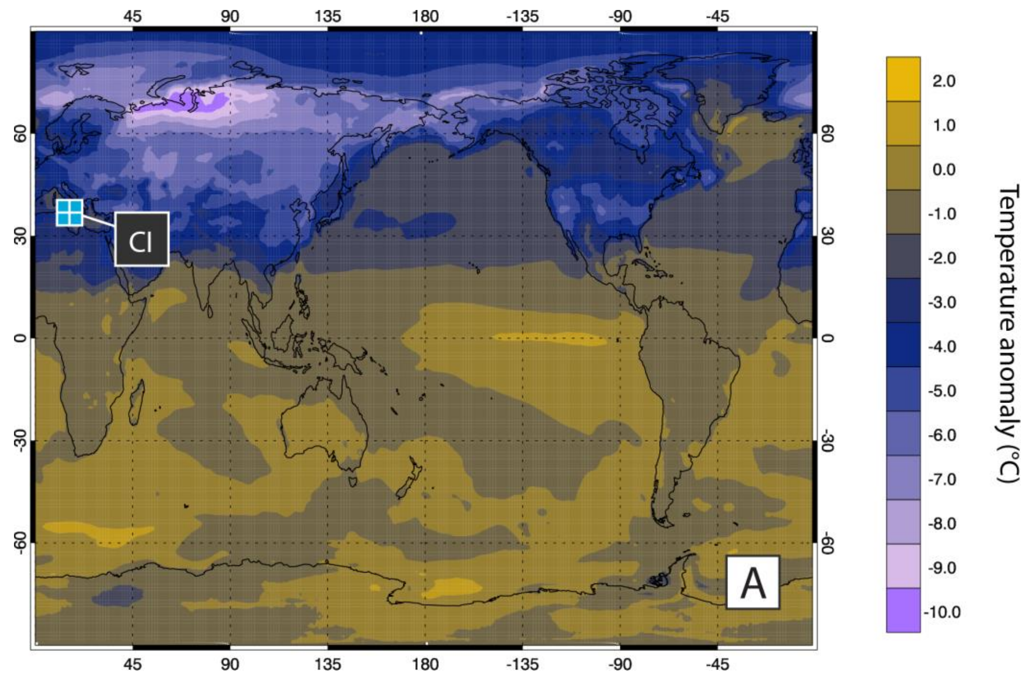

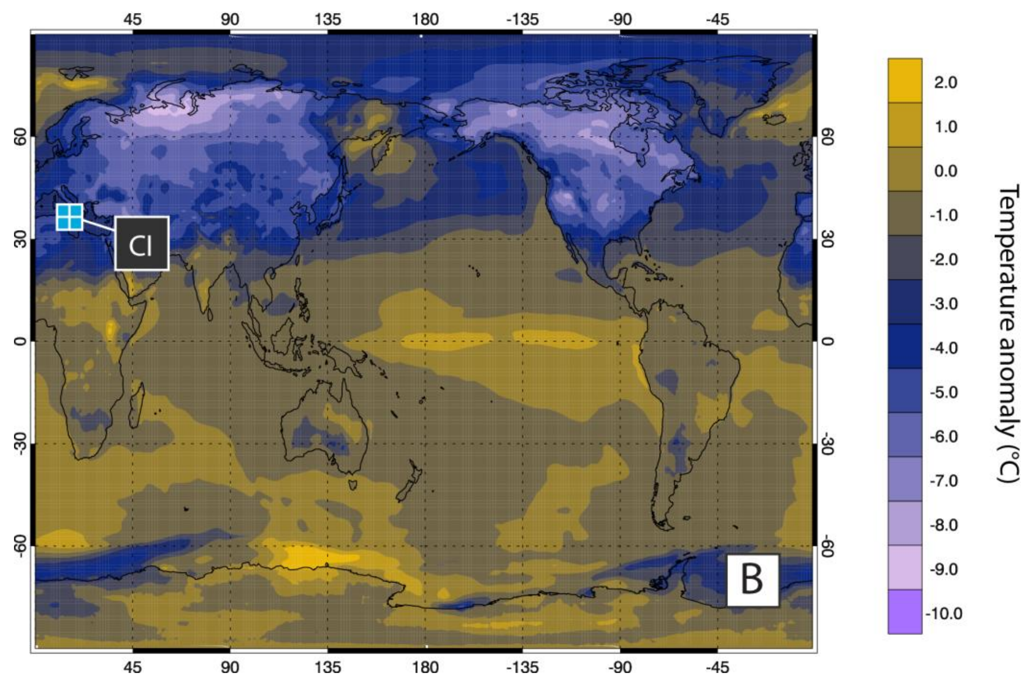

Figure S3. Sensitivity test comparing: S2A. Temperature anomalies for the 200 Tg SO_2 ensemble runs (as shown in Figure 3B) versus S2B. Temperature anomalies for a 200 Tg SO_2 run initialized with present-day climate and geography. The temperature anomalies are averaged during the first year after the eruption. While temperature changes vary in North America, the consistent decrease in the magnitude of temperature anomalies from Eastern to Western Europe supports the robustness of our conclusions.

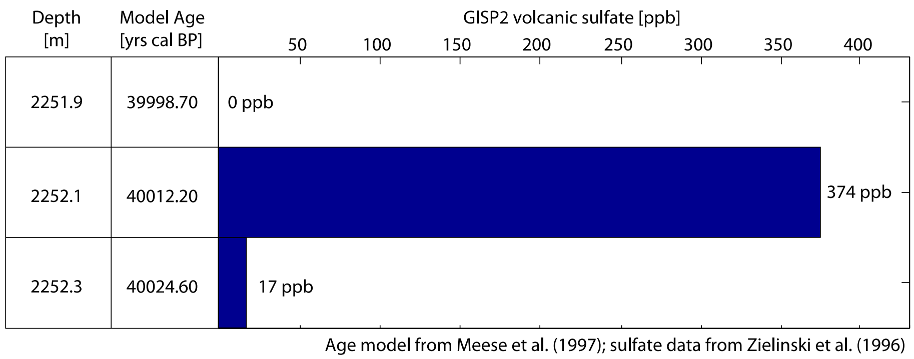

Figure S4. The volcanic sulfate peak at 2252.1 meters depth in the GISP2 core that has been attributed to the Campanian Ignimbrite eruption.

References Cited

Aquila, V., Oman, L.D., Stolarski, R.S., Colarco, P.R., and Newman, P.A., 2012, Dispersion of the volcanic sulfate cloud from a Mount Pinatubo–like eruption: Journal of Geophysical Research: Atmospheres (1984–2012), v. 117, no. D6.

Argus, D.F., and Peltier, W.R., 2010, Constraining models of postglacial rebound using space geodesy: a detailed assessment of model ICE-5G (VM2) and its relatives: Geophysical Journal International, v. 181, no. 2, p. 697-723.

Banks, W.E., d'Errico, F., Peterson, A.T., Kageyama, M., Sima, A., and Sánchez-Goñi, M., 2008, Neanderthal extinction by competitive exclusion: PLoS One, v. 3, no. 12, p. e3972.

Brady, E.C., Otto-Bliesner, B.L., Kay, J.E., and Rosenbloom, N., 2013, Sensitivity to Glacial Forcing in the CCSM4.: Journal of Climate, v. 26, no. 6.

Collins, W.D., Rasch, P.J., Boville, B.A., et al., 2006, The formulation and atmospheric simulation of the Community Atmosphere Model version 3 (CAM3): Journal of Climate, v. 19, no. 11, p. 2144-2161.

English, J.M., Toon, O.B., and Mills, M.J., 2013, Microphysical simulations of large volcanic eruptions: Pinatubo and Toba: Journal of Geophysical Research: Atmospheres, v. 118, no. 4, p. 1880-1895.

English, J., Toon, O., Mills, M., and Yu, F., 2011, Microphysical simulations of new particle formation in the upper troposphere and lower stratosphere: Atmos.Chem.Phys, v. 11, no. 17, p. 9303-9322.

Fedele, F.G., Giaccio, B., and Hajdas, I., 2008, Timescales and cultural process at 40,000 BP in the light of the Campanian Ignimbrite eruption, Western Eurasia: Journal of human evolution, v. 55, no. 5, p. 834-857.

Gent, P.R., Danabasoglu, G., Donner, L.J., et al., 2011, The Community Climate System Model Version 4.: Journal of Climate, v. 24, no. 19.

Higham, T., Douka, K., Wood, R., et al., 2014, The timing and spatiotemporal patterning of Neanderthal disappearance: Nature, v. 512, no. 7514, p. 306-309.

Hurrell, J.W., Holland, M., Gent, P., et al., 2013, The community earth system model: a framework for collaborative research: Bulletin of the American Meteorological Society, v. 94, no. 9, p. 1339-1360.

Lambeck, K., Purcell, A., Zhao, J., and SVENSSON, N., 2010, The Scandinavian ice sheet: from MIS 4 to the end of the Last Glacial Maximum: Boreas, v. 39, no. 2, p. 410-435.

Marsh, D.R., Mills, M.J., Kinnison, D.E., Lamarque, J., Calvo, N., and Polvani, L.M., 2013, Climate change from 1850 to 2005 simulated in CESM1 (WACCM): Journal of Climate, v. 26, no. 19, p. 7372-7391.

Martrat, B., Grimalt, J.O., Lopez-Martinez, C., et al., 2004, Abrupt temperature changes in the Western Mediterranean over the past 250,000 years: Science (New York, N.Y.), v. 306, no. 5702, p. 1762-1765.

Meese, D., Gow, A., Alley, R., et al., 1997, The Greenland Ice Sheet Project 2 depth- age scale: Methods and results: Journal of Geophysical Research: Oceans (1978–2012), v. 102, no. C12, p. 26411-26423.

Mills, M.J., Toon, O.B., Turco, R.P., Kinnison, D.E., and Garcia, R.R., 2008, Massive global ozone loss predicted following regional nuclear conflict: Proceedings of the National Academy of Sciences of the United States of America, v. 105, no. 14, p. 5307-5312.

Murray, L.T., Mickley, L.J., Kaplan, J.O., Sofen, E.D., Pfeiffer, M., and Alexander, B., 2014, Factors controlling variability in the oxidative capacity of the troposphere since the Last Glacial Maximum: Atmospheric Chemistry and Physics, v. 14, no. 7, p. 3589-3622.

Neely, R., Toon, O., Solomon, S., et al., 2013, Recent anthropogenic increases in SO2 from Asia have minimal impact on stratospheric aerosol: Geophysical Research Letters, v. 40, no. 5, p. 999-1004.

Neely, R.R., English, J.M., Toon, O.B., Solomon, S., Mills, M., and Thayer, J.P., 2011, Implications of extinction due to meteoritic smoke in the upper stratosphere: Geophysical Research Letters, v. 38, no. 24.

Niemeier, U., Timmreck, C., Graf, H., Kinne, S., Rast, S., and Self, S., 2009, Initial fate of fine ash and sulfur from large volcanic eruptions: Atmospheric Chemistry and Physics, v. 9, no. 22, p. 9043-9057.

Schmidt, G.A., and Shindell, D.T., 2003, Atmospheric composition, radiative forcing, and climate change as a consequence of a massive methane release from gas hydrates: Paleoceanography, v. 18, no. 1.

Smith, R., Jones, P., Briegleb, B., et al., 2010, The Parallel Ocean Program (POP) reference manual: Ocean component of the Community Climate System Model (CCSM): Los Alamos National Laboratory, LAUR-10-01853.

Tabazadeh, A., Toon, O.B., Clegg, S.L., and Hamill, P., 1997, A new parameterization of H2SO4/H2O aerosol composition: Atmospheric implications: Geophysical Research Letters, v. 24, no. 15, p. 1931-1934.

Tarasov, L., and Peltier, W.R., 2004, A geophysically constrained large ensemble analysis of the deglacial history of the North American ice-sheet complex: Quaternary Science Reviews, v. 23, no. 3, p. 359-388.

Toohey, M., Krüger, K., Niemeier, U., and Timmreck, C., 2011, The influence of eruption season on the global aerosol evolution and radiative impact of tropical volcanic eruptions: Atmospheric Chemistry and Physics, v. 11, no. 23, p. 12351-12367.

Toon, O., Turco, R., Westphal, D., Malone, R., and Liu, M., 1988, A multidimensional model for aerosols: Description of computational analogs: Journal of the Atmospheric Sciences, v. 45, no. 15, p. 2123-2144.

Turco, R., Hamill, P., Toon, O., Whitten, R., and Kiang, C., 1979, A one-dimensional model describing aerosol formation and evolution in the stratosphere: I. Physical processes and mathematical analogs: Journal of the Atmospheric Sciences, v. 36, no. 4, p. 699-717.

Zielinski, G.A., Mayewski, P.A., Meeker, L.D., Whitlow, S., and Twickler, M.S., 1996, A 110,000-yr record of explosive volcanism from the GISP2 (Greenland) ice core: Quaternary Research, v. 45, no. 2, p. 109-118.